IVYSPRING INTERNATIONAL PUBLISHER

Theranostics

2016; 6(8): 1096-1104. doi: 10.7150/thno.14361

Research Paper

Fabrication of Graphene and AuNP Core Polyaniline Shell Nanocomposites as Multifunctional Theranostic Platforms for SERS Real-time Monitoring and Chemo-photothermal Therapy

Haolin Chen, Zhiming Liu✉, Songyang Li, Chengkang Su, Xuejun Qiu, Huiqing Zhong and Zhouyi Guo✉

MOE Key Laboratory of Laser Life Science & SATCM Third Grade Laboratory of Chinese Medicine and Photonics Technology, College of Biophotonics, South China Normal University, Guangzhou 510631, Guangdong, China.

✉ Corresponding authors: Dr. Zhiming Liu and Prof. Zhouyi Guo, Telephone and fax: 86-20-85211428 E-mail: liuzm@scnu.edu.cn (Dr. Z.M. Liu) ann@scnu.edu.cn (Prof. Z.Y. Guo).

Received: 2015.11.10; Accepted: 2016.03.09; Published: 2016.04.28

Abstract

In this work, novel theranostic platforms based on graphene oxide and AuNP core polyaniline shell (GO-Au@PANI) nanocomposites are fabricated for simultaneous SERS imaging and chemo-photothermal therapy. PANI, a new NIR photothermal therapy agent with strong NIR absorption, outstanding stability and low cytotoxicity is decorated on AuNPs by one-pot oxidative polymerization, then the Au@PANI core-shell nanoparticles are attached to the graphene oxide (GO) sheet via π-π stacking and electrostatic interaction. The obtained GO-Au@PANI nanohybirds exhibit excellent NIR photothermal transduction efficiency and ultrahigh drug-loading capacity. The nanocomposites can also serve as novel NIR SERS probes utilizing the intense SERS signals of PANI. Rapid SERS imaging of cancer cells is achieved using this ultrasensitive nanoprobe. GO-Au@PANI also reveals good capability of drug delivery with the DOX-loading efficiency of 189.2% and sensitive NIR/pH-responsive DOX release. The intracellular real-time drug release dynamics from the nanocomposites is monitored by SERS-fluorescence dual mode imaging. Finally, chemo-photothermal ablation of cancer cells is carried out in vitro and in vivo using GO-Au@PANI as high-performance chemo-photothermal therapeutic nanoagent. The theranostic applications of GO-Au@PANI endow it with great potential for personalized and precise cancer medicine.

Key words: Graphene, Au nanoparticles, Polyaniline, SERS imaging, Chemo-photothermal therapy.

Introduction

Graphene, a newly developed material, and its derivatives have recently captured tremendous focus due to their unique properties in various fields including biomedicine [1, 2]. In terms of cancer treatment, graphene sheet could serve as an ideal burgeoning support for efficient drug loading, taking advantage of its large specific surface area available [3, 4]. The demonstration of using graphene oxide (GO) in drug delivery was first initiated by Dai group in 2008 [4]. Utilizing its high near-infrared (NIR) absorbance, nano-graphene has also been used as a photothermal agent for in vivo cancer treatment with encouraging therapeutic outcomes [5-8]. Our group utilized DOX-loaded PEGylated nano-graphene oxide to facilitate combined chemotherapy and photothermal therapy (PTT) in mouse xenografts, which showed a synergistic cancer therapeutic effect of chemo-photothermal therapy for the first time [9].

GO has shown effective therapeutic effect to cancer, but it also shows low photothermal

conversion efficiency. The appearance of abundant functional groups makes it easy to be modified. It has been decorated by a variety of nanocomposites, such as gold nanorods (GNRs) [10, 11], gold nanoparticles (AuNPs) [12], semiconductor copper sulfide nanoparticles [13], to enhanced photothermal energy conversion. Among them, gold-based nanomaterials received the most attention, owing to the phenomenon of surface plasmon resonance and their tunable optical property [14-17]. However, the gold nanoparticles are always troubled with the biotoxicity and they have low photostability under long-term laser irradiation [18]. In addition, the preparation of some Au nanostructures with NIR photothermal conversion properties usually need precise synthesis conditions. Some unifunctional therapeutic nanoagents are also limited in their theranostic applications. Thus, the alternatives with easy preparation, good photostability and multifunctionality are still in demand.

Recently, conducting polymer (CP) materials, such as polypyrrole (PPy), poly-(3,4-ethylene dioxythiophene): poly(4-styrenesulfonate) (PEDOT/PSS) and polyaniline (PANI), which have been widely used for electronic, optical and electrochemical applications, gear towards application in PTT. Due to their strong NIR absorption, outstanding stability and low cytotoxicity, they have been reported to show photothermal effect for ablation of cancer cells in vitro and in vivo [19-22]. Among these CP materials, PANI is one of the most useful conducting polymers because of its conductivity, mechanical flexibility, and low cost [23]. PANI can also be used to wrap metal nanometerials in order to reduce the toxicity of metal and improve the conversion efficiency at the same time [24, 25]. In our latest work, we demonstrated the GNR-PANI core-shell nanoparticles for high-performance photothermal cancer therapy [26]. Interestingly, the core-shell nanostructures could also serve as novel ultrasensitive surface-enhanced Raman scattering (SERS) nanoprobes due to the excellent SERS signals of PANI after fabricating on the surface of GNRs via one-pot oxidative polymerization. In comparison with the traditional gold-based SERS probes [24, 27-28], the fabrication of GNR-PANI core-shell nanoparticles was easily manipulated and low-cost.

Herein, we report the GO and Au@PANI nanocomposites for SERS imaging and chemo-photothermal cancer ablation. AuNP@PANI core-shell nanoparticles are firstly synthesized by assembling PANI onto the surface of gold nanosturctures through facile in situ oxidative polymerization; then the obtaining Au@PANI nanostructures are deposited on the polyvinylpyrrolidone-stabilized GO (GO-PVP) sheet via π-π stacking and electrostatic interaction. The GO-Au@PANI nanocomposites show promising SERS imaging capability of tumor cells and outstanding chemo-photothermal performance for cancer therapy, which reveal their theranostic potential in nanomedicine.

Results and Discussion

Characterization of GO-Au@PANI

The GO nanosheet was functionalized with PVP before fabrication of graphene-metal nanocomposites. The atomic force microscope (AFM) image of GO-PVP illustrated that the nanosheet was almost single layered with the average thickness of about 1.3 nm (Fig. S1). The morphology of the obtained GO-Au@PANI was investigated by the transmission electron microcopy (TEM). It can be observed that a large amount of Au nanoparticles with spherial or strip-like shape are deposited on the flake-like GO nanostructure (Fig. 1B). The generation of AuNPs can also be confirmed by the energy dispersive X-ray (EDX) analysis (Fig. S2). Fig. 1C shows the TEM image of GO-Au@PANI at a higher magnification where an encapsulation matrix consist of PANI appears outside the metal nanoparticles, forming core-shell like nanostructures. An insert high-resolution image clearly identify the three components (Au, PANI and GO) of the hybrids with different contrasts, verifying the successful fabrication of GO-Au@PANI. The sizes of the nanocomposites was measured by the dynamic light scattering analysis, which displayed a mean dimension of 120 nm (Fig. S3). The UV-vis-NIR spectrum of Au@PANI (Fig. 1D) shows the absorption peaks at 345, 438 and 792 nm, indicating the formation of PANI [29]. The longitudinal SPR absorption of PANI red-shifted to 816 nm after attached onto the GO sheet, which is consistent with the morphological changes observed in the TEM image. The Raman spectra of the nanomaterials are given in Fig. 1E. Two prominent peaks at 1344 cm^{-1} (D band) and 1594 cm^{-1} (G band) are observed in the Raman spectrum of GO sheet which can be attributed to the disordered graphite edge and graphite lattice, respectively. In comparison with the normal Raman specturm of PANI, extraordinarily intense SERS signals assigned to the molecular vibration of PANI emerge in the Raman spectrum of Au@PANI under NIR laser excitation (785 nm) [30]. This inherent SERS feature endows it with promising potential for bioimaging. In the Raman spectral line of GO-Au@PANI, some characteristic peaks ascribed to PANI (1168 cm^{-1}) and GO (1598 cm^{-1}) respectively can be observed, indicating that the nanocomposites has be sucessfully

synthesized. The conjugation of Au@PANI with GO-PVP can also be proved by the FTIR spectra (Fig. S4). In addition, the GO-Au@PANI nanohybrids exhibit excellent stability in water, phosphate buffered saline (PBS) buffer and RPMI-1640 medium (Fig. S5) and outstanding photostability (Fig. S6).

The strong NIR photoabsorption of GO-Au@PANI in UV-vis-NIR absorbance spectrum motivated us to investigate the temperature elevation induced by NIR laser irradiation. Different concentrations of GO-Au@PANI were exposed to a continuous-wave fiber-coupled diode laser (808 nm, 2.5 W cm^{-2}) for 5 min. As shown in Fig. 2A, the temperature of GO-Au@PANI aqueous solution show a rapid temperature rise in marked contrast to the pure water sample, demonstrating that the photothermal heating effect could increase monotonically with the GO-Au@PANI concentration. It can be concluded that the GO-Au@PANI possesses good photothermal performance, which can rapidly convert near-infrared laser light energy into heat. The results illustrate that GO-Au@PANI is promising as an ideal NIR-light absorber for cancer photothermal therapy.

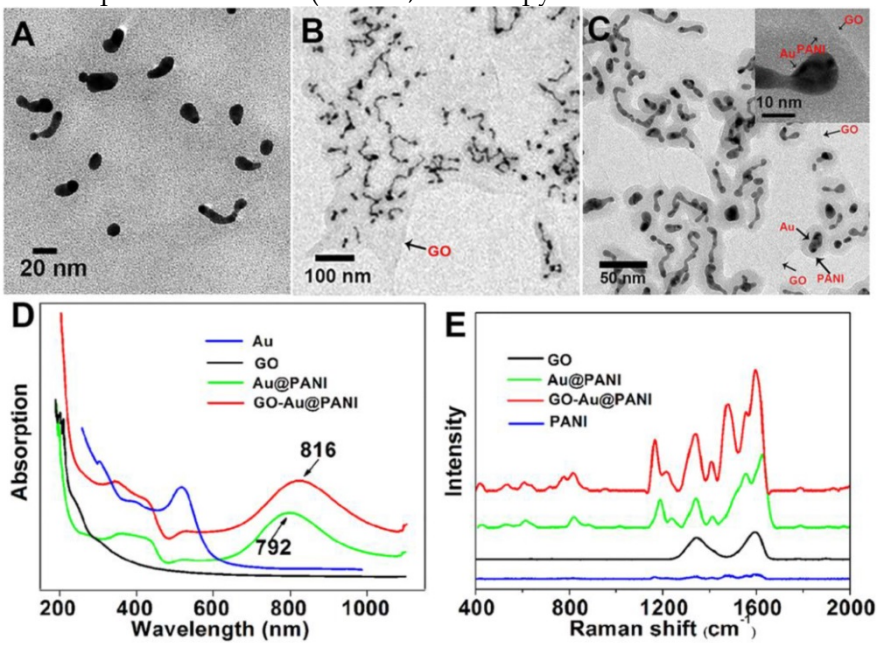

Figure 1. The TEM images of Au@PANI A) and GO-Au@PANI with different resolutions B) and C), the UV-vis-NIR absorbance spectra D) and the Raman spectra of the nanostructures E).

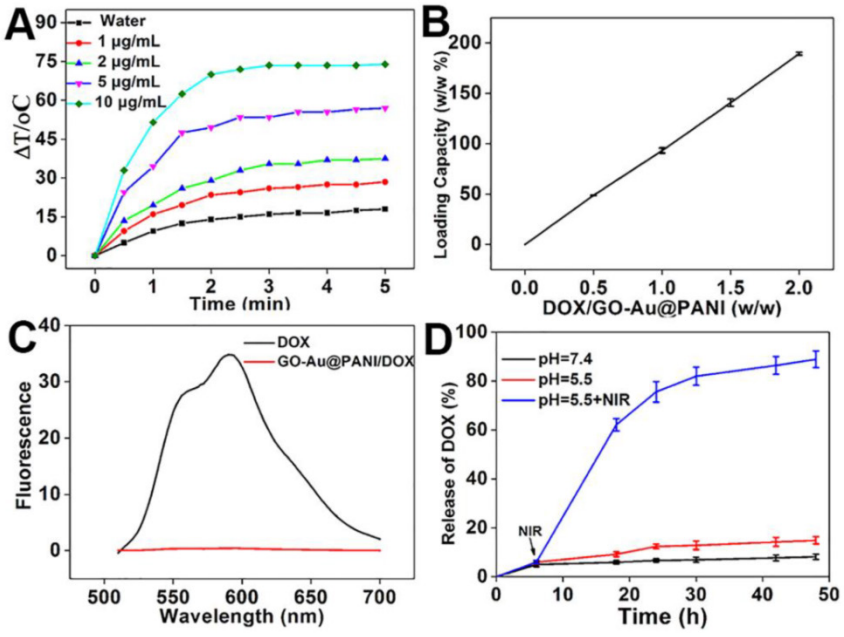

Figure 2. A) NIR-induced heat generation of different concentrations of GO-Au@PANI aqueous dispersion. B) Quantification of DOX loading at various DOX concentrations. C) Fluorescence spectra of GO-Au@PANI/DOX and free DOX at the same concentration of DOX. D) DOX release profiles from GO-Au@PANI/DOX in PBS buffer at pH values of 7.4 and 5.5 with or without laser irradiation (2.5 W cm^{-2}, 10 min).

Drug loading and release on GO-Au@PANI

Graphene and their derivatives with ultrahigh surface area have been extensively reported as efficient nanocarriers for drug delivery [4, 31]. The capability of GO-Au@PANI for drug delivery was carried out using DOX as the durg model. The amount of DOX loaded on the GO nanosheets improves in an initial DOX concentration-dependent manner, showing the maximal loading efficiency of 189.2% (Fig. 2B). The adsorption of DOX on GO-Au@PANI may be attributed to the hydrophobic interaction and π-π stacking. In addition, the fluorescence signal of GO-Au@PANI/DOX is drastically quenched by GO, which can be attributed to the fluorescence resonance energy transfer between DOX and the nanocarrier (Fig. 2C). An efficient drug delivery system should have not only a high drug-loading capacity but also a sustained DOX release formulation. The released DOX from GO-Au@PANI was collected and then measured by fluorescence spectroscopy. DOX-releasing characteristic from GO-Au@PANI/DOX is shown in Fig. 2D. The lower pH values in PBS solutions, the more DOX molecules are released, but the amount of drug released is still comparatively low after a 48 h incubation. Noteworthy, the release rate of DOX from GO-Au@PANI nanosheets can be significantly improved with the aid of NIR laser irradiation; about 90% of DOX is released 2 d after 808 nm laser exposure (2.5 W cm^{-2}, 10 min). It is likely that the local heating may induce increased thermal vibration thus loosening the drug molecule from GO-Au@PANI.

SERS imaging of tumor cells

Molecular imaging using fluorescence-based techniques is often limited by the photobleaching of fluorescent molecules, autofluorescence from the biological samples and large spectral overlap between broadband fluorescence dyes [32-34]. Raman scattering provides information about the unique vibrational modes of molecules with narrow spectral bandwidth and is resistant to photobleaching and autofluorescence, which maybe a good alternative to the fluorescence imaging [35, 36]. SERS imaging of cancer cells was performed using GO-Au@PANI as the nanoprobe. The SERS images of 4T1 mammary carcinoma cells were acquired using the distinct SERS signal of PANI at 1100-1200 cm^{-1}. As shown in Fig. 3A, the intense SERS signals of PANI suffuse the cancer cell, and the SERS image is closely correlated with the bright-field image. The two Raman spectral lines extracted from the cytoplasm and nucleus regions indicate that the nanoprobes are situated almost exclusively in the cytoplasm. To understand the cell internalization process of the GO-Au@PANI, we conducted the SERS mapping experiments of 4T1 cells incubated with GO-Au@PANI for 0.5 h, 1 h, 2 h, 4 h and 8 h. As shown in Fig. 3B, the cells incubated with GO-Au@PANI for 0.5 h and 1 h yield obscure Raman signals, which suggest that the time is too short for a large amount of GO-Au@PANI to enter into the cells. The SERS image of 4T1 cells becomes distinct after 2 h incubation with the nanocomposites. Bright and clear-cut SERS image can be observed at 4 h, showing more GO-Au@PANI nanohybrids are taken up by the cancer cells. The amount of intracellular GO-Au@PANI are maintained at a considerable degree after 8 h of incubation, when the 4T1 cells are still filled with the strong SERS signals ascribed to the GO-Au@PANI nanoprobes.

Dynamics studying Intracellular drug drug delivery

The promising SERS activity of GO-Au@PANI facilitates the dynamics studying of intracellular drug delivery. The real-time drug release process was monitored by a SERS-fluorescence spectroscopy, where the SERS signals (1100-1200 cm^{-1}, λ_{ex}: 785 nm) of the nanocarrier and the fluorescent signals (590-640 nm, λ_{ex}: 514 nm) of DOX can be collected simultaneously. The green false-color images in Fig. 4 show the SERS signal distribution of the GO-Au@PANI nanocarrier in 4T1 cells. It can be seen that the intracellular SERS signals stay constant in the cytoplasmic region during a 45 min observation, demonstrating that the drug loading does not affect the intracellular behavior of nanovehicles. Fig. 4B displays the fluorescent image of DOX just entering into the cancer cells, where the photoluminescent signals are very weak owing to the fluorescence quenching effect of the GO nanosheet. Moreover, the fluorescent image is highly overlapped with the SERS image of the nanocarrier (Fig. 4A), also showing that the drug has not yet released from GO-Au@PANI. Real-time fluorescence mapping of DOX was then performed every 15 min. It can be noticed that the fluorescent signals escalate along with the increasing incubation time and reach a peak at 45 min, which reveals a releasing process of DOX from the nanovehicles. The distribution of DOX also changes after detachment, and the drug tends to gather in the nucleus with the time increasing. Almost all the fluorescent signals are detected in the nucleus, the target of DOX, at 45 min (Fig. 4E), while the nanocarriers remain in the cytoplasm (Fig. 4F).

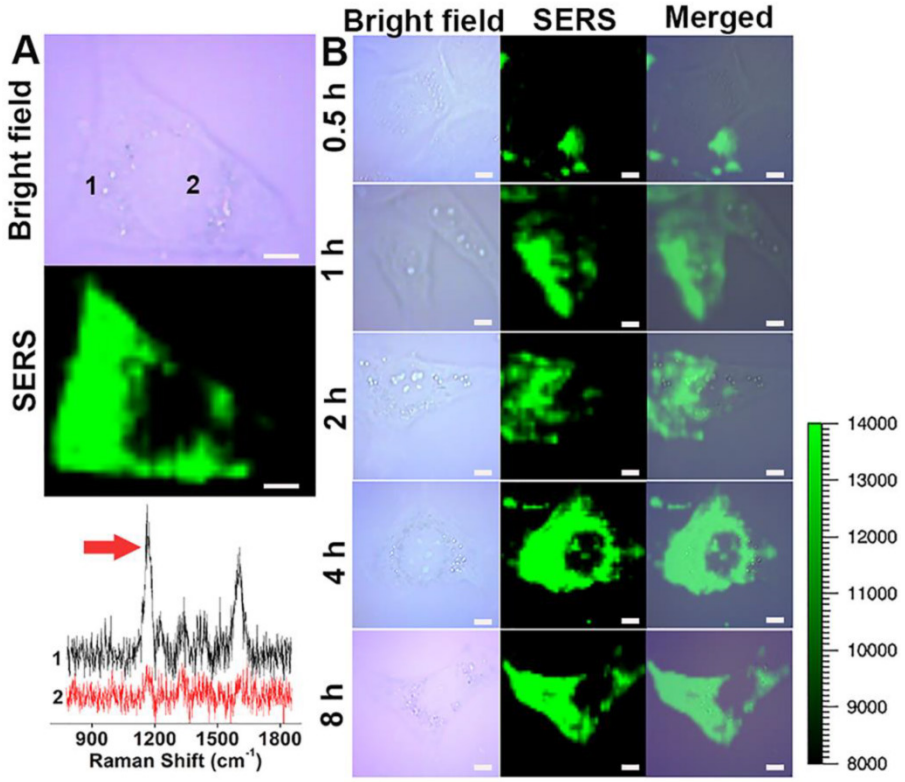

Figure 3. NIR SERS imaging of cancer cells using GO-Au@PANI as the nanoprobe. A) Bright field microscopic image and SERS image of a 4T1 cell after incubation GO-Au@PANI for 8 h. The black and red lines represent the SERS spectra of two different spots marked in cytoplasmic and nuclear, respectively (scale bar: 5 μm). B) NIR SERS images of 4T1 cells incubated with GO-Au@PANI for 0.5, 1, 2, 4 and 8 h, respectively (scale bar: 10 μm). The arrow indicates the Raman peak used for SERS mapping.

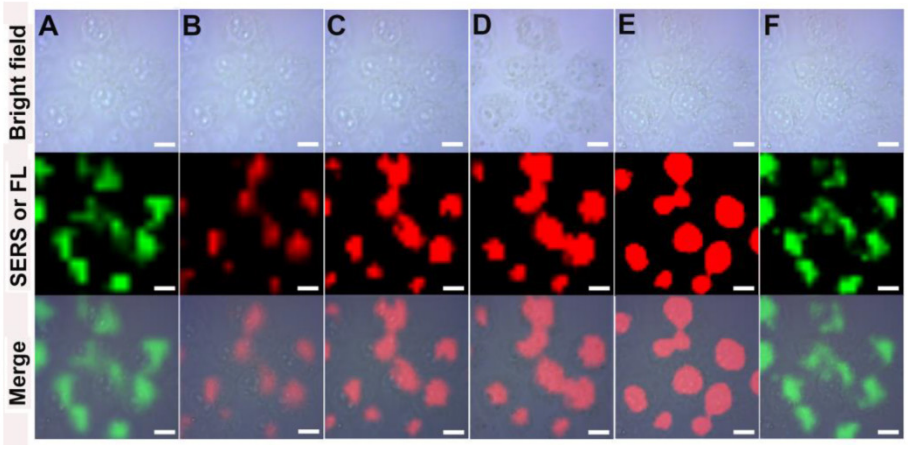

Figure 4. The intracellular real-time drug release dynamics monitored by SERS-fluorescence dual mode imaging. The SERS and fluorescence mapping were performed at 0 min A) and B), 15 min C), 30 min D), 45 min E) and F) (scale bar: 10 μm). SERS mapping A) and F) was conducted using the SERS bands of PANI at 1100-1200 cm^{-1} under 785 nm laser excition and the fluorescence imaging B), C), D) and E) was performed using the fluorescent signals of DOX at 590-640 nm under 514 nm laser excition.

Cytotoxicity assessments of SERS nanotags

For further biomedical application, the cytotoxicity of GO-Au@PANI was investigated by the classic methyl thiazolyl tetrazolium (MTT) assay. The GO-Au@PANI nanocomposites were diluted with RPMI-1640 medium and incubated with 4T1 tumor cells in 5% CO_2 at 37 °C for 24 h. It is found that the GO-Au@PANI reveal no obvious toxic effect on 4T1 cells at concentrations below 50 μg mL^{-1} (Fig. 5A), showing a good biocompatibility. We next evaluated the *in vitro* chemo-photothermal efficacy of DOX loaded GO-Au@PANI by conducting the MTT assay. As shown in Fig. 5B, dose-dependent anti-proliferative effects are observed in the tumor cells after various treatments. Compared with DOX, GO-Au@PANI/DOX exhibits relatively weak cytotoxicity at the same drug concentration, which can be ascribed with the low release efficiency of GO-Au@PANI without laser irradiation. The cell ablation effect of GO-Au@PANI is significantly improved by the NIR laser exposure, which induces

about 77.4% cell death at the concentration of 5 μg mL^{-1}. In comparison with other treatments, the chemo-photothermal treatment reaches the strongest therapeutic effect, which can be attributed to the combined cell-killing effect initiated by the drug and heat. The synergistic effect is more pronounced at the drug concentrations below 3 μg mL^{-1}. For example, the inhibition rate of tumor cells treated with chemo-photothermal is 79.8% (Group V, 3 μg mL^{-1}), much higher than that of cells treated with DOX (Group III, 39.2%) or GO-Au@PANI (Group IV, 42.1%). To further identify the cell viability, the cells were incubated at 37 °C for another 24 h after laser irradiation and then stained by Hoechst 33258 (nuclear marker). Fig. 5C shows the representative fluorescence microscope images of 4T1 cells treated with various treatments. The amount of apoptotic cells treated with GO-Au@PANI/DOX which are observed as the irregular granules with bright blue luminescence are much more than that in the 4T1 cells with other treatments. The remarkable cell-killing capability of GO-Au@PANI/DOX is expected to reduce drug dose, making it a promising approach to overcome resistance to chemotherapeutic agents in tumor therapy.

In vivo cancer therapeutic efficacy

Finally, the *in vivo* synergistic therapeutic efficacy of GO-Au@PANI/DOX was investigated using Balb/c mouse as the model. An infrared thermal camera was used to record the temperature change in the tumor area under NIR irradiation. It is noticed that no obvious surface temperature change emerges on the tumor region injected with PBS (Group II) during the NIR irradiation (Fig. 6A). In marked contrast, remarkable temperature increasing are observed in the tumor sites injected with the nanostructures (ΔT ≈ 55 °C), confirming the promising pothothermal potential of GO-Au@PANI. The tumor growth curves after various treatments are shown in Fig. 6B, where the tumors of mice treated with DOX experience an equivalent growth rate in comparison with that of control groups during the 16-day observation period, demonstrating that the dosage of administered DOX is inadequate to inhibit the tumor growth. However, the *in vivo* anti-tumor effect of GO-Au@PANI is extraordinarily obvious. The tumors in Group IV and Group V are effectively eliminated with only small black scars left at the tumor sites (Fig. S7). Compared with the tumors with photothermal treatment, the relative tumor volume in Group V is much smaller (Fig. 6C, D), showing a better therapeutic efficacy. The microscopic images of tumors with various treatments were also acquired using hematoxylin and eosin (H&E) staining analysis. As noticed in Fig. 6E, the normal tumor cells with regular morphology and intact cell nucleus [37, 38], are largely observed in control groups. As excepted, most tumor cells are severely destroyed after chemo-photothermal treatment, which is in good agreement with the previous data, further confirming the superior anti-cancer therapeutic efficacy of the combination therapy. The improved therapeutic efficacy of GO-Au@PANI/DOX plus NIR laser treatment may be attributed to synergistic effect of PTT and chemotherapy. On the one hand, local hyperthermia can cause direct cell killing as the result of protein denaturing and aggregation or indirect killing due to the triggering of programmed cell death [39, 40]. On the other hand, the sensitive pH/NIR-triggered DOX release initiates an efficient nuclear-targeted drug killing of the tumor cells.

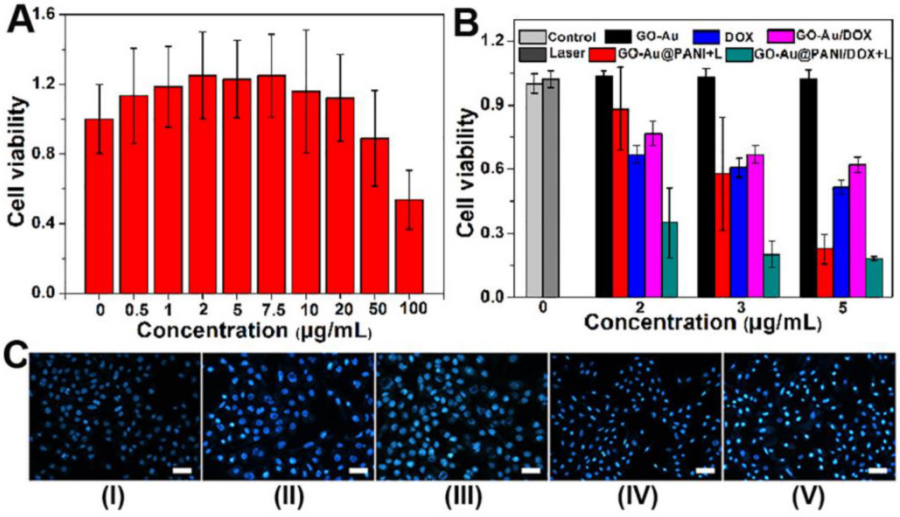

Figure 5. *In vitro* chemo-photothermal ablation of tumor cells. A) Relative cell viability of 4T1 cells exposed to different concentrations of GO-Au@PANI for 24 h. B) Relative viability of 4T1 cells after various treatments at the same DOX concentrations. The data represent the means of triplicate measurements. All data are presented as mean±SD. C) Fluorescence photomicrographs of the 4T1 cells after various treatments (Group I: control, Group II: control+laser, Group III: DOX, Group IV: GO-Au@PANI+laser, Group V: GO-Au@PANI/DOX+laser) and staining with Hoechst 33258 (scale bar: 100 μm).

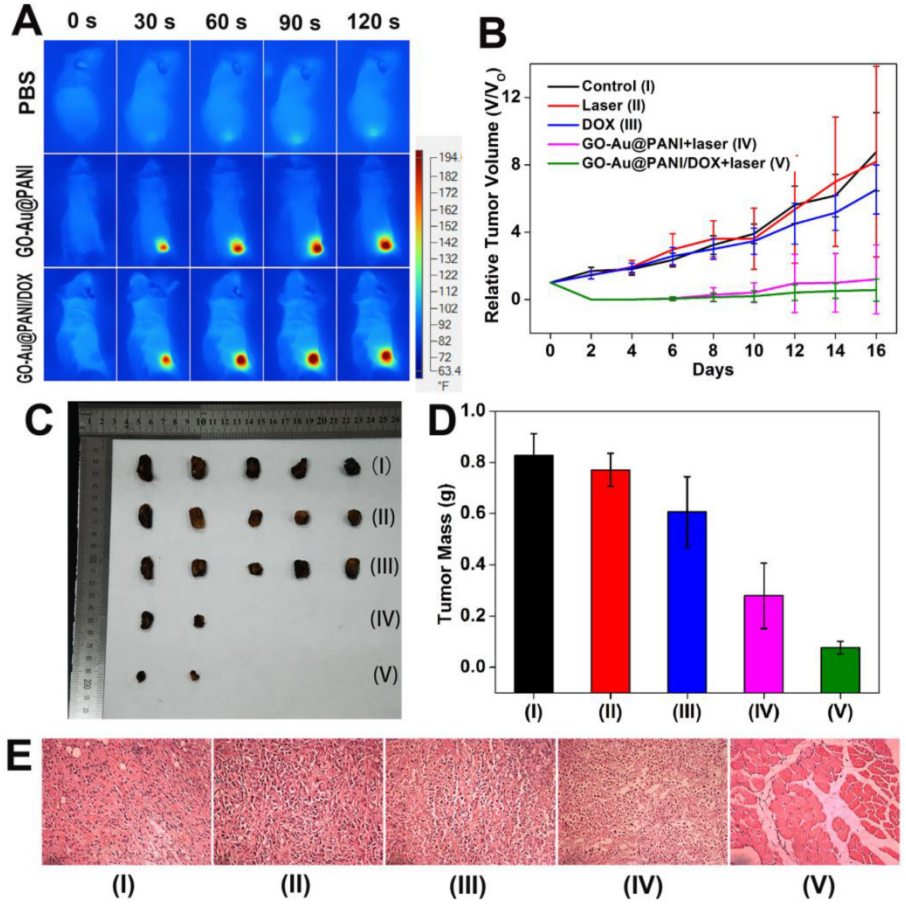

Figure 6. A) Infrared thermal images of 4T1-tumor-bear mice after injection with PBS (I), GO-Au@PANI (IV) and GO-Au@PANI/DOX (V) (1 mg kg^{-1}) under laser irradiation (808 nm, 2.5 W cm^{-2}) at different time intervals. B) Tumor growth curves of different groups of mice during the treatments. C) Photographs of the tumors collected from different groups of mice at the end of treatments (day 16). D) Average weights of tumors collected from mice. E) Representative H&E-stained tumor slice images from mice post various treatments (Group I: control, Group II: control+laser, Group III: DOX, Group IV: GO-Au@PANI+laser, Group V: GO-Au@PANI/DOX+laser, scale bar: 200 μm).

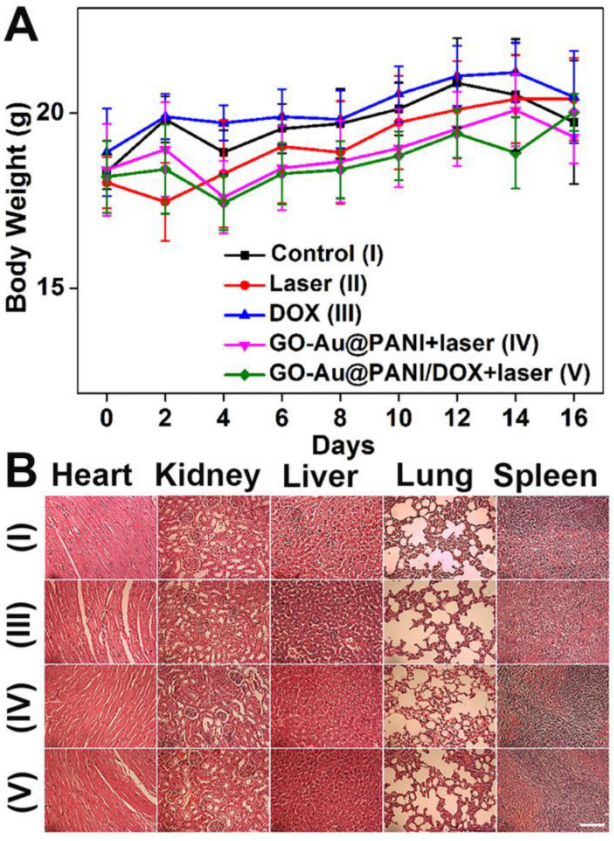

In addition, toxic side effects have always been of great concern in the development of nanomedicine. The body weight of the mice was monitored after treatment because high toxicity often causes weight loss. The curves of body weight changes are displayed in Fig. 7A, where no significant body weight losses are noted in all groups. Histology analysis of major organs from mice 16 days after treatment indicates that neither noticeable organ damage nor inflammation is associated with various treatments (Fig. 7B). Moreover, the blood samples were gathered from the mice for blood analysis. The liver function markers (alkaline phosphatase, alanine aminotransferase, and aspartate aminotransferase) and kidney function marker (blood urea nitrogen) are measured to be normal (Fig. S8), suggesting no evident renal and hepatic disorder of mice induced by the treatments. Therefore, these results reveal that the GO-Au@PANI based chemo-photothermal therapy induces no significant side effect to the tumor-bearing mice.

Figure 7. A) Mean body weights of mice in various groups. B) Micrographs of H&E stained organ slices acquired at 16 days post-treatment (Group I: control , Group III: DOX, Group IV: GO-Au@PANI+laser, Group V: GO-Au@PANI/DOX+laser, scale bar: 200 μm).

Conclusion

In summary, we have successfully fabricated biocompatible graphene and AuNP core polyaniline shell nanocomposites for biomedical applications for the first time. The GO-Au@PANI nanocomposites show good biocompatibility, outstanding stability, strong NIR absorbance high drug loading efficiency and sensitive NIR/pH-responsive drug releasing capacity, which promote the practical application of GO-Au@PANI for high-performance chemo-photothermal therapy *in vitro* and *in vivo*. The nanohybrids also reveal excellent NIR SERS activity, which have been served as the ultra-sensitive nanoprobes for rapid SERS imaging of cancer cells. Real-time monitoring of intracellular drug release from GO-Au@PANI has then been carried out using SERS-fluorescence dual mode imaging. Further investigation should pay attention to the long-term systemic toxicity of graphene-based nanostructures. The fabrication of these multifunctional theranostic platforms for integrated SERS real-time monitoring and chemo-photothermal therapy which can be an efficient strategy for imaging-guided cancer therapy.

Supplementary Material

Supplementary figures.
http://www.thno.org/v06p1096s1.pdf

Acknowledgements

This work is supported by the National Natural Science Foundation of China (61335011, 61275187 and 21505047), Specialized Research Fund for the Doctoral Program of Higher Education of China (20114407110001 and 20134407120003), the Natural Science Foundation of Guangdong Province of China (2014A030310306 and 2014A030311024), the Science and Technology Project of Guangdong Province of China (2012A080203008), the Science and Technology Innovation Project of the Education Department of Guangdong Province of China (2013KJCX0052), and the Scientific Research Cultivation Fund for Young Teachers of South China Normal University (14KJ10).

Competing Interests

The authors have declared that no competing interest exists.

References

1. Hu SH, Chen YW, Hung WT, Chen IW, Chen SY. Quantum-dot-tagged reduced graphene oxide nanocomposites for bright fluorescence bioimaging and photothermal therapy monitored in situ. Adv Mater. 2012; 24: 1748-54.
2. Qian J, Wang D, Cai FH, Xi W, Peng L, Zhu ZF, et al. Observation of multiphoton-induced fluorescence from graphene oxide nanoparticles and applications in in vivo functional bioimaging. Angew Chem Int Edit. 2012; 51: 10570-5.
3. Sun XM, Liu Z, Welsher K, Robinson JT, Goodwin A, Zaric S, et al. Nano-graphene oxide for cellular Imaging and drug delivery. Nano Res. 2008; 1: 203-12.
4. Liu Z, Robinson JT, Sun X, Dai HJ. PEGylated nanographene oxide for delivery of water-insoluble cancer drugs. J Am Chem Soc. 2008; 130: 10876-7.
5. Li M, Yang XJ, Ren JS, Qu KG, Qu XG. Using graphene oxide high near-infrared absorbance for photothermal treatment of Alzheimer's disease. Adv Mater. 2012; 24: 1722-8.
6. Yang K, Wan JM, Zhang S, Tian B, Zhang YJ, Liu Z. The influence of surface chemistry and size of nanoscale graphene oxide on photothermal therapy of cancer using ultra-low laser power. Biomaterials. 2012; 33: 2206-14.
7. Yang K, Zhang S, Zhang G, Sun X, Lee ST, Liu Z. Graphene in mice: ultrahigh in vivo tumor uptake and efficient photothermal therapy. Nano Lett. 2010; 10: 3318-23.
8. Feng LZ, Liu Z. Graphene in biomedicine: opportunities and challenges. Nanomedicine-UK. 2011; 6: 317-24.
9. Zhang W, Guo ZY, Huang DQ, Liu ZM, Guo X, Zhong HQ. Synergistic effect of chemo-photothermal therapy using PEGylated graphene oxide. Biomaterials. 2011; 32: 8555-61.
10. Dembereldorj U, Choi SY, Ganbold EO, Song NW, Kim D, Choo J, et al. Gold nanorod-assembled PEGylated graphene-oxide nanocomposites for photothermal cancer therapy. Photochem Photobiol. 2014; 90: 659-66.
11. Moon H, Kumar D, Kim H, Sim C, Chang J-H, Kim J-M, et al. Amplified photoacoustic performance and enhanced photothermal stability of reduced graphene oxide coated gold nanorods for sensitive photoacoustic imaging. ACS nano. 2015; 9: 2711-9.
12. Zedan AF, Moussa S, Terner J, Atkinson G, El-Shall MS. Ultrasmall gold nanoparticles anchored to graphene and enhanced photothermal effects by laser irradiation of gold nanostructures in graphene. ACS Nano. 2012; 7: 627-36.
13. Bai J, Liu YW, Jiang X. Multifunctional PEG-GO/CuS nanocomposites for near-infrared chemo-photothermal therapy. Biomaterials. 2014; 35: 5805-13.
14. Chou CH, Chen CD, CR W. Highly Efficient, Wavelength-tunable, gold nanoparticle based optothermal nanoconvertors. J Phy Chem B. 2005; 109: 11135-8.
15. Huang X, Jain PK, El-Sayed IH, El-Sayed MA. Plasmonic photothermal therapy (PPTT) using gold nanoparticles. Lasers Med Sci. 2008; 23: 217-28.
16. Link S, El-Sayed MA. Size and Temperature Dependence of the plasmon absorption of colloidal gold nanoparticles. J Phys Chem B. 1999; 103: 4212-7.
17. Zhang JZ. Biomedical applications of shape-controlled plasmonic nanostructures: a case study of hollow gold nanospheres for photothermal ablation therapy of cancer. J Phys Chem Lett. 2010; 1: 686-95.
18. Botha TL, James TE, Wepener V. Comparative aquatic toxicity of gold nanoparticles and ionic gold using a species sensitivity distribution approach. J Nanomater. 2015; 501: 986902.
19. Zhou J, Lu ZG, Zhu XJ, Wang XJ, Liao Y, Ma ZF, et al. NIR photothermal therapy using polyaniline nanoparticles. Biomaterials. 2013; 34: 9584-92.
20. Cheng L, Yang K, Chen Q, Liu Z. Organic stealth nanoparticles for highly effective in vivo near-infrared photothermal therapy of cancer. ACS nano. 2012; 6: 5605-13.
21. Chen M, Fang XL, Tang SH, Zheng NF. Polypyrrole nanoparticles for high-performance in vivo near-infrared photothermal cancer therapy. Chem Commun. 2012; 48: 8934-6.
22. Zha ZB, Yue XL, Ren QS, Dai ZF. Uniform polypyrrole nanoparticles with high photothermal conversion efficiency for photothermal ablation of cancer cells. Adv Mater. 2013; 25: 777-82.
23. Li D, Huang JX, Kaner RB, Richard B, Kaner. Polyaniline nanofibers: a unique polymer nanostructure for versatile applications. Acc Chem Res. 2009; 42: 135-45.
24. Lu WT, Singh AK, Khan SA, Senapati D, Yu HT, Ray PC. Gold nano-popcorn-based targeted diagnosis, nanotherapy treatment, and in situ monitoring of photothermal therapy response of prostate cancer cells using surface-enhanced Raman spectroscopy. J Am Chem Soc. 2010; 132: 18103-14.
25. Abel SB, Molina MA, Rivarola CR, Kogan MJ, Barbero CA. Smart polyaniline nanoparticles with thermal and photothermal sensitivity. Nanotechnology. 2014; 25: 495-602.
26. Liu ZM, Ye BG, Jin M, Chen HL, Zhong HQ, Wang XP, et al. Dye-free near-infrared surface-enhanced Raman scattering nanoprobes for bioimaging and high-performance photothermal cancer therapy. Nanoscale. 2015; 7: 6754-61.
27. Wang XJ, Wang C, Cheng L, Lee ST, Liu Z. Noble metal coated single-walled carbon nanotubes for applications in surface enhanced Raman scattering imaging and photothermal therapy. J Am Chem Soc. 2012; 134: 7414-22.
28. Zhang Y, Qian J, Wang D, Wang YL, He SL. Multifunctional gold nanorods with ultrahigh stability and tunability for in vivo fluorescence imaging, SERS detection, and photodynamic therapy. Angew Chem Int Ed. 2013; 52: 1148-51.
29. Li DX, Cui Y, Wang KW, He Q, Yan XH, Li JB. Thermosensitive nanostructures comprising gold nanoparticles grafted with block copolymers. Adv Funct Mater. 2007; 17: 3134-40.
30. Mallick K, Witcomb MJ, Dinsmore A, Scurrell MS. Polymerization of aniline by auric acid: formation of gold decorated polyaniline nanoballs. Macromol Rapid Commun. 2005; 26: 232-5.
31. Liu Z, Sun XM, Nakayama-Ratchford N, Dai HJ. Supramolecular chemistry on water-soluble carbon nanotubes for drug loading and delivery. ACS nano. 2007; 1: 50-6.
32. Aubin J. Autofluorescence of viable cultured mammalian cells. J Histochem Cytochem. 1979; 27: 36-43.

33. Song L, Hennink E, Young IT, Tanke HJ. Photobleaching kinetics of fluorescein in quantitative fluorescence microscopy. Biophys J. 1995; 68: 2588-2600.
34. Haraguchi T, Shimi T, Koujin T, Hashiguchi N, Hiraoka Y. Spectral imaging fluorescence microscopy. Genes Cells. 2002; 7: 881-7.
35. Zavaleta C, De La Zerda A, Liu Z, Keren S, Cheng Z, Schipper M, et al. Noninvasive Raman spectroscopy in living mice for evaluation of tumor targeting with carbon nanotubes. Nano Lett. 2008; 8: 2800-5.
36. Keren S, Zavaleta C, Cheng Z, de la Zerda A, Gheysens O, Gambhir SS. Noninvasive molecular imaging of small living subjects using Raman spectroscopy. P Natl Acad Sci USA. 2008; 105: 5844-9.
37. Chao W, Xu H, Chao L, Liu YM, Li ZW, Yang GB, et al. Iron oxide @ polypyrrole nanoparticles as a multifunctional drug carrier for remotely controlled cancer therapy with synergistic antitumor effect. ACS nano. 2013; 7: 6782-95.
38. Liu B, Chen YY, Li CX, He F, Hou ZY, Huang SS, et al. Poly(Acrylic Acid) modification of Nd3+-sensitized upconversion nanophosphors for highly efficient UCL imaging and pH-Responsive drug delivery. Adv Funct Mater. 2015; 25: 4717-29.
39. Gabai VL, Meriin AB, Yaglom JA, Volloch VZ, Sherman MY. Role of Hsp70 in regulation of stress-kinase JNK: implications in apoptosis and aging. FEBS Lett. 1998; 438: 1-4.
40. Mukhopadhaya A, Mendecki J, Dong XY, Liu LB, Kalnicki S, Garg M, et al. Localized hyperthermia combined with intratumoral dendritic cells induces systemic antitumor immunity. Cancer Res. 2007; 67: 7798-806.